

LARGE-EDDY SIMULATION OF KATABATIC FLOW

Simon L. Axelsen

University of Utrecht, the Netherlands

1

1 Introduction

The interaction between the atmosphere and the earth's surface takes place in the boundary layer (BL), which compared to the free atmosphere, has a high turbulence intensity. During the night time, or the polar winter, the boundary layer is often stably stratified, whereby buoyancy reduces the turbulence intensity. In the stable boundary layer (SBL), the only production of turbulence is through shear, which plays a predominant role near the surface. Although being reduced in intensity by buoyancy, turbulence is still an important transport and mixing mechanism for heat, momentum and energy in the SBL. Despite the fact that energy in the SBL is partly transported by waves (Nappo, 2002), we will in this text not consider this transport mechanism. In case of a stably stratified boundary layer over a sloping surface, gravity is an accelerating term in the along-slope momentum equation. That is, if an air parcel near the surface is cooled, it becomes heavier than its surroundings and starts to descend down the slope. A density driven down-slope flow, often called a katabatic flow, can thus arise without any external forcing, and is frequently directed along the fall line of the slope. Moreover, a typical wind speed profile in a katabatic regime exhibits a wind maximum.

Glaciers, small in lateral extent and frequently located at higher latitudes, are sensitive to climate fluctuations. Melting is a process which is very sensitive to air temperature variations, and the observed retreat in valley glaciers during the last century is an evidence of this sensitivity (Oerlemans, 1994). Although melting of glaciers

is mainly caused by solar radiation (Greuell *et al.*, 1997), measurements on glacier surfaces show that turbulent fluxes contribute 25% to 40% to the total energy balance, see Denby (2002) and references herein.

Traditionally, there are two types of analytical descriptions of katabatic flow. The first type of model considers local equilibria in the heat and momentum equations, which allows for an analytical solution that describes the vertical profiles of e.g. the velocity and temperature in the katabatic layer. Hereafter, we will refer to this type of model as a 'profile model'. The first of such was presented by Prandtl (1942), who in the heat equation assumed a local equilibrium between adiabatic downslope warming and cooling by slope-normal heat flux divergence in a stratified background atmosphere; in the momentum equation acceleration by gravity is opposed surface friction. The solution gives vertical profiles of the down-slope velocity and the temperature deficit Δ , which is defined as the temperature of the air minus the background temperature. The Prandtl model produces a velocity profile inhibiting a wind maximum, and the temperature deficit profile shows a maximum near the surface and a decrease with height.

Later, Grisogono and Oerlemans (2001a) (hereafter GO) noted that because the Prandtl model assumes constant turbulence exchange coefficient the sharp gradients in the velocity and temperature profiles obtained from measurements are not reproduced. They pointed out that if the temperature profile is correct, the wind is wrong and vice versa. GO extended the classical Prandtl model to solve the katabatic flow problem using gradually varying, height dependent turbulence exchange coefficients and constant but arbitrary Prandtl number. Despite the fact that in the GO-model the flow dependent turbulence exchange coefficients have to be determined *a priori*, it was found that this model was better at reproducing observations

¹Corresponding author address: Simon L. Axelsen, Institute for Marine and Atmospheric Research Utrecht, Princetonplein 5, NL - 3584 CC Utrecht, email: s.l.axelsen@uu.nl

than the classical Prandtl model. In subsequent studies by Grisogono and Oerlemans (2001b) and Parmhed *et al.* (2004) it was also found that the GO-model was capable of reproducing the surface fluxes of heat and momentum inferred from observations. Grisogono (2003) later extended the GO-model to include time dependence, and more recently also the effect of the earth's rotation (Kavcic and Grisogono, 2007). Gutman and Malbakhov (1964), and Shapiro and Fedorovich (2008) describe analytical models also including the Coriolis force, which over the large ice sheets of Greenland and Antarctica becomes important (Van den Broeke *et al.*, 2002), but will not be discussed in further detail here.

The second type of analytical models, the hydraulic models, is based on the assumption that bulk quantities such as mass flux, can be related to each other using a closed system of equations, and that details in the vertical profiles are of lesser importance (Haiden and Whiteman, 2005). The hydraulic model type was supported by calculations of Papadopoulos *et al.* (1997), who analysed data from an array of meteorological stations on Mt. Hymettos, Greece. They found that in the katabatic layer bulk quantities of wind and temperature, calculated by vertical integration, compared well with theoretical models.

The immediate benefit of hydraulic model type over the profile models described above, is that they permit changes in bulk quantities with down-slope distance. Moreover, numerical weather prediction and climate models have a resolution too coarse to resolve the detailed fields of the katabatic flow, and thus use parameterizations based on hydraulic models (Haiden and Whiteman, 2005).

In the hydraulic model by Manins and Turner (1978), who extended the work of Fleagle (1950), it was assumed that all the fluid participating in the katabatic flow was entrained from the environment; the entrainment rate was specified *a priori* through parameterization based on laboratory experiments and related field experiments. Nappo and Rao (1987), however, pointed out that parameterizations used by Manins and Turner would not necessarily be applicable to katabatic flows under all ambient

conditions. Instead of investigating katabatic flow using a highly parameterized analytical model, Nappo and Rao used a time-dependent, two-dimensional numerical model based on turbulent kinetic energy closure. The model used a slope-following coordinate system and the flow considered was down a uniform open slope with a finite length. The numerical model provided down-slope velocity and temperature as function of down-slope distance and height. These variables could be vertically integrated to yield values for the entrainment rate needed by analytical hydraulic models.

Whereas Nappo and Rao applied the 1.5-order turbulent kinetic energy closure proposed by Delage (1974), Denby (2002) more recently studied katabatic flow using a one-dimensional model that applied second-order closure. He argued that 1.5-order closure used in several earlier numerical models, depend on horizontally homogeneous and vertically monotonous stable boundary layers, which may be incompatible with conditions in the katabatic flow. The second-order closure model required parameterization of the the viscous dissipation of momentum and heat, the turbulent transport and the pressure-strain/temperature correlations. Denby carried out simulations of katabatic flow using input data from three measurement campaigns, and showed that the model was capable of reproducing both mean profiles and flux measurements when the flow was almost one-dimensional and the turbulence locally determined. An important finding was that at the height of the wind maximum, where shear production goes to zero, the turbulence transport term becomes important

Whereas Denby successfully simulated mean fields and turbulent fluxes of a katabatic flow using second-order closure, there has in literature also been a call for numerical studies using the techniques of large-eddy simulation (Grisogono and Oerlemans, 2001b; Parmhed *et al.*, 2004). The concept of large-eddy simulation (LES) is that the larger scale turbulent motion is resolved explicitly, whereas small scale turbulence is understood to be isotropic and can be parameterized using turbulence theory. Pope (2000) provides an introduction to the techniques of LES, for a more comprehensive

description see Sagaut (1998); Geurts (2004). LES of the convective boundary layer has been done since the mid seventies, but simulation of the turbulent flow in the SBL requires a much finer resolution (Beare *et al.*, 2006), which has only recently become possible with the increase in computer power. Moreover, there has only been a few large-eddy simulations of the SBL over a sloping surface. Skillingstad (2003) used LES with a rotated coordinate system, applied periodic boundary conditions on the sides but open boundary condition on the top and bottom of the slope. To ensure conservation of mass, the mass flux at the slope top was adjusted to balance the mass flux exiting at the slope bottom. The initial ambient atmosphere was neutrally stratified, and the simulation was carried out until the slope flow velocity and turbulent fluxes reached a near-equilibrium state over the central portion of the slope. Skillingstad mainly investigated the importance of the ambient cross slope wind on the katabatic flow, and his analysis of the momentum budget showed that near the surface the flow is maintained by a balance between downslope buoyancy forcing and vertical turbulence flux from surface drag. Above the wind maximum, he found that the flow acceleration due to buoyancy is retarded by horizontal advection of slower moving ambient air. Skillingstad also noted a seemingly self-similar behaviour of the momentum budget profiles as the cross wind component was increased. For a given cross-slope wind the turbulence kinetic energy budget showed that the main source of turbulence production was through shear, which was balanced by dissipation through friction and buoyancy. An increase in the cross-normal wind would yield an increase in the shear production term and corresponding balances. The peak value of the shear production would also move closer to the surface.

Skillingstad considered katabatic flow over a steep (20°) and a shallow (1°) slope, and in this article we will focus on katabatic flow over moderately steep slopes ($\sim 5^\circ$). To this end, we will use results from LES, but in contrast to Skillingstad the slope is regarded to be infinitely long. Details on the numerical model is given in the next section, and in Section 3

model output is compared to observations. To our knowledge, no LES study of katabatic flow has considered the effects of stratification and cooling rate on the flow, which will be the focus of Section 4. Although the emphasis will be on mean characteristic profiles and scaling thereof, we will also show profiles of turbulent fluxes of momentum and heat.

2 LES model

The governing equations of katabatic flow are described in a reference frame aligned with the topographical gradient. The reference frame has been rotated by the slope-angle α ($\alpha > 0$) with respect to the z^* axis, which points in the opposite direction of the gravity vector \mathbf{g} . The velocity components parallel and normal to the surface, e.g. in the x and z directions, are denoted by u and w , respectively. The ambient atmosphere is stably stratified and its potential temperature is in the *non*-rotated coordinate system denoted by $\theta_a(z^*)$. The corresponding lapse rate of the ambient atmosphere is constant, $\gamma \equiv \frac{d\theta_a}{dz^*}$. The Brunt-Väisälä frequency $N = \sqrt{g\gamma/T_0}$ and T_0 is a reference temperature. In the rotated reference frame, the filtered model equations for momentum and buoyancy, using the Einstein summation convention (e.g. Riley *et al.*, 1997) are respectively

$$\begin{aligned} \frac{d\bar{u}_i}{dt} &= -\frac{\partial \bar{\pi}}{\partial x_i} - 2\epsilon_{ijk}\Omega_j\bar{u}_k \\ &- \bar{b}[\delta_{i1}\sin\alpha - \delta_{i3}\cos\alpha] - \frac{\partial \tau_{ij}}{\partial x_j}, \end{aligned} \quad (1)$$

$$\frac{d\bar{b}}{dt} = -N^2[\bar{u}_1\sin\alpha - \bar{u}_3\cos\alpha] - \frac{\partial \tau_{bj}}{\partial x_j} \quad (2)$$

where variables with an overbar denote filtered quantities and sub-filter scale (SFS) quantities are denoted by a prime. The three filtered velocity components are denoted \bar{u}_i , the filtered buoyancy is $\bar{b} = g\bar{\Delta}/T_0$ where $\bar{\Delta}$ is as defined above, and δ_{ij} is the Kronecker Delta function. Note that in the text we will use the terms buoyancy and heat interchangeably. In the buoyancy equation the term including the slope-angle α is the advection of ambient temperature. The

modified pressure and sub-filter scale stresses and buoyancy flux τ_{ij} and τ_{bj} are given by

$$\begin{aligned}\bar{\pi} &= \frac{\bar{p}}{\rho_0} + \frac{2}{3}\bar{e}, \\ \tau_{ij} &= \overline{u_i u_j} - \bar{u}_i \bar{u}_j - \frac{2}{3}\bar{e}\delta_{ij} \quad \text{and} \quad (3) \\ \tau_{bj} &= \overline{u_j b} - \bar{u}_j \bar{b}\end{aligned}$$

respectively. In the SFS model - sometimes labelled a TKE model (e.g. Beare *et al.*, 2006) or a Deardorff type model after Deardorff (1980) - the SFS turbulent kinetic energy (TKE) $\bar{e} = \frac{1}{2}(\overline{u_k u_k} - \bar{u}_k \bar{u}_k)$ is a prognostic variable governed by

$$\frac{d\bar{e}}{dt} = -\tau_{ij} \frac{\partial \bar{u}_i}{\partial x_j} + \tau_{b3} - c_\epsilon \frac{e^{3/2}}{\lambda}, \quad (4)$$

where $c_\epsilon = \frac{2\pi}{c_f} (3C_k/2)^{-3/2} = 0.93$, $c_f = 2$, and the Kolmogorov constant $C_k = 1.5$, values as in Pope (2000). In Equation 4 we have assumed that the contribution from the horizontal component of the SFS buoyancy flux is negligible. The SFS fluxes of heat and momentum in Equations (3) and (4) are modelled according to:

$$\begin{aligned}\tau_{ij} &= -K_m^s \left(\frac{\partial \bar{u}_i}{\partial x_j} + \frac{\partial \bar{u}_j}{\partial x_i} \right) \\ \tau_{b3} &= -K_b^s \frac{\partial \bar{b}}{\partial z},\end{aligned}$$

where $K_m^s = c_m \lambda \sqrt{\bar{e}}$ and $K_b = (1 + 2\lambda/\delta)K_m$ are the SFS exchange coefficients of respectively momentum and buoyancy (Raasch and Etling, 1991); $c_m = c_\epsilon \pi^{-2} = 0.094$ is a dimensionless constant (Dosio, 2005). The values of the constant c_ϵ , c_f and c_m are evaluated from inertial subrange theory assuming that the spectral cut-off wave number $k_c = \pi/\lambda$ is lying in the inertial subrange. In all simulations we use $\lambda = \delta$, where δ is the numerical grid size. To prevent laminarization, in the lowest 10% of the domain we let the filter width decrease² linearly to $\lambda = \delta/2$ at the surface. In the wall layer, between the solid surface and the first grid point, we use standard Monin-Obukhov (MO) theory (Foken, 2006) despite its limitations (Mahrt, 1998, 1999).

²Analogous to the van Driest damping function (e.g. Pope, 2000)

The most important input parameters are the slope-angle, the background stratification, and the surface buoyancy flux. All simulations use an equidistant grid, the ratio of the grid distance in the horizontal to the vertical is ~ 6 . A ratio different from unity will introduce extra numerical errors, but is used for numerical efficiency. The time integration is performed using a third order Runge-Kutta scheme. The advection term produces the most numerical dissipation, which can be reduced by using a higher order scheme; here we use a sixth order central difference scheme. Lastly, in the top 25% of the domain, there is a sponge layer that removes fluctuations of velocity temperature in order to dissipate gravity waves before they can reflect at the model top (Cuijpers, 1994; Khairoutdinov and Randall, 2003).

3 Observations and model validation

In the summer of 1994 a glacio-meteorological experiment on the Pasterze glacier in Austria was performed (PASTEX). The experiment consisted of mast measurements at six different locations and balloon soundings; for the model validation we will only use data from the mast at site A1. Wind and temperature were measured at eight levels (0.25, 0.5, 1, 2, 4, 6, 8, and 13 m), whereas fluxes of momentum and heat were measured at two levels (2.5 and 10.3 m). Details on the measurement sites and instrumentation are given in Van den Broeke (1997).

For our comparison we look at nocturnal data (half-hour measurements averaged over the period 22 - 04 h) measured during a single night with only small synoptic disturbances. The surface heat flux is obtained by linear extrapolation of the observed heat flux: $\overline{w\theta}_s = -0.035 \text{ K ms}^{-1}$. The roughness length was 4.4 mm. The horizontal domain and grid distance are 250 m and 2.7 m, respectively, and in the vertical direction 51 m and 0.4 m, respectively.

We first consider the time evolution of the flow; unlike SBLs over flat surfaces, katabatic flows become steady after some time, but in an os-

cillatory way. Schumann (1990) showed for an up-slope boundary flow (convective counterpart of katabatic flow) that the vertically averaged temperature deficit and velocity oscillate with a time-period

$$\tau = \frac{2\pi}{N \sin \alpha}.$$

Figure 1(a) shows the oscillatory behaviour of the vertically averaged velocity UD and temperature deficit TD (defined below). At first the surface cools, whereby the flow is accelerated. With increasing wind speeds, more potentially warm air is advected down-slope, which reduces the temperature deficit. The flow is retarded as the temperature deficit decreases, but with a weak flow, the surface cooling increases again. Figure 1(b) shows the down-slope velocity at four different heights and also the vertically averaged velocity $UD \equiv h^{-1} \int_0^h u dz$; for simplicity we have taken h to be the top of the domain. It is seen that the velocity near the surface starts increasing before the velocity further away from the surface. At $z = 1$ m the velocity becomes more or less constant after $t/\tau = 0.4$, whereas at other heights the oscillation continues until $t/\tau \sim 2$. The velocities at 1 and 5 m show a sudden drop around $t/\tau \sim 0.2$, numerical instability is a possible cause, but we have not found a more concrete explanation. The damping is stronger than in Schumann (1990) who introduced artificial damping to reduce computer time needed to reach a steady state solution. Moreover, direct numerical simulation of moderately turbulent katabatic flow (Fedorovich, personal communication) has shown an oscillation in UD also for $t/\tau \gtrsim 10$, which contradicts the damping. We can only speculate as to what the cause of the damping may be, but a comparison with simulations using other input parameters suggests that the damping increases foremost with decreasing stratification, and increases with increasing surface heat flux.

In the remainder we assume a stationary state obtained by averaging the model results over the oscillation period $t/\tau = 2 - 3$. Moreover, mean profiles are evaluated by averaging the resultant fields over planes parallel to the surface. Figure 2 shows model results together with observations of the downslope wind speed, the ver-

tical momentum flux, the temperature deficit³, and the vertical heat flux. To assess the measurement error, we have calculated the standard deviation of the wind and temperature at each level, using the half hour measurements.

The shape of the wind profile strongly resembles the observations, and although the model overestimates the wind maximum u_{max} , it is still within the error-bars. The modelled momentum flux also seem to fit the observations to a good degree; near the surface the modelled \overline{uw} is slightly overestimated. Larger discrepancies are found between modelled and observed temperature deficit. Near the surface the modelled values and observations agree, but for $z > 2$ the modelled temperature deficit is too large. Figure 2 also indicates that the height at which $\overline{\Delta}$ goes to zero is too high. e.g. the boundary layer height is overestimated, which is also seen in the temperature flux profile. The surface heat flux was one of the input parameters to the numerical model, which is why the modelled and observed heat flux at $z \sim 2$ m should agree. However, at $z \sim 10$ m, the modelled heat flux is about 2.5 times the observed heat flux. i.e. there is too much mixing of heat whereby the BL grows.

Denby (2002) also compared model results with data from Pasterze, but instead of using data from a single night, he averaged the observations from a 12-day period characterised by weak synoptic conditions. From his figure 3, it would appear the his modelled heat flux compares better to the observations than our results, but a close inspection of his heat flux at ~ 10 m gives $\overline{w\theta} \sim -0.022$ Kms⁻¹ (our comparison value: -0.095), which is very similar to our model output. If we slightly change the interval over which the observations are averaged, the discrepancy between modelled and observed heat flux becomes smaller, but the differences between modelled and observed velocity and momentum flux becomes larger. This raises the question of how to select data for comparison, which we will not attempt to answer. However, based on the results shown in this section we are confident that our numerical model can capture the main features of a katabatic flow.

³In this section only, we revert to the notation of temperature (deficit) to give a more intuitive comparison with observations

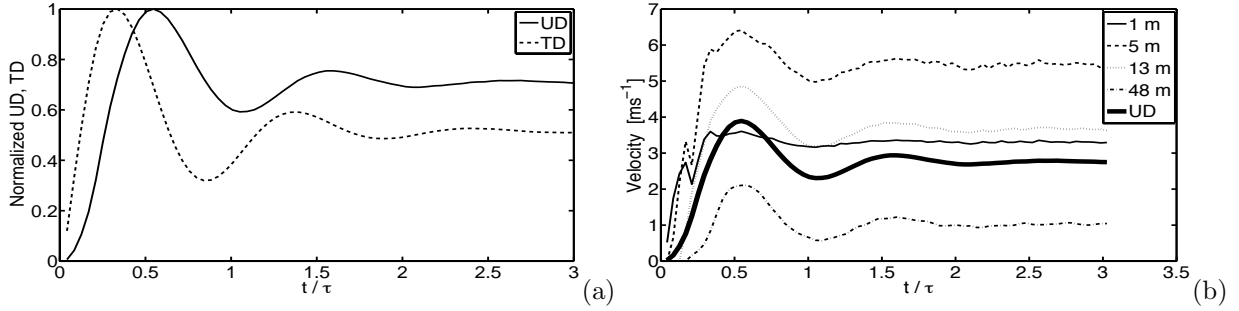


Figure 1: (a) Vertically averaged velocity UD and temperature deficit TD as function of non-dimensional time, and (b) the time evolution of the down-slope velocity at different heights.

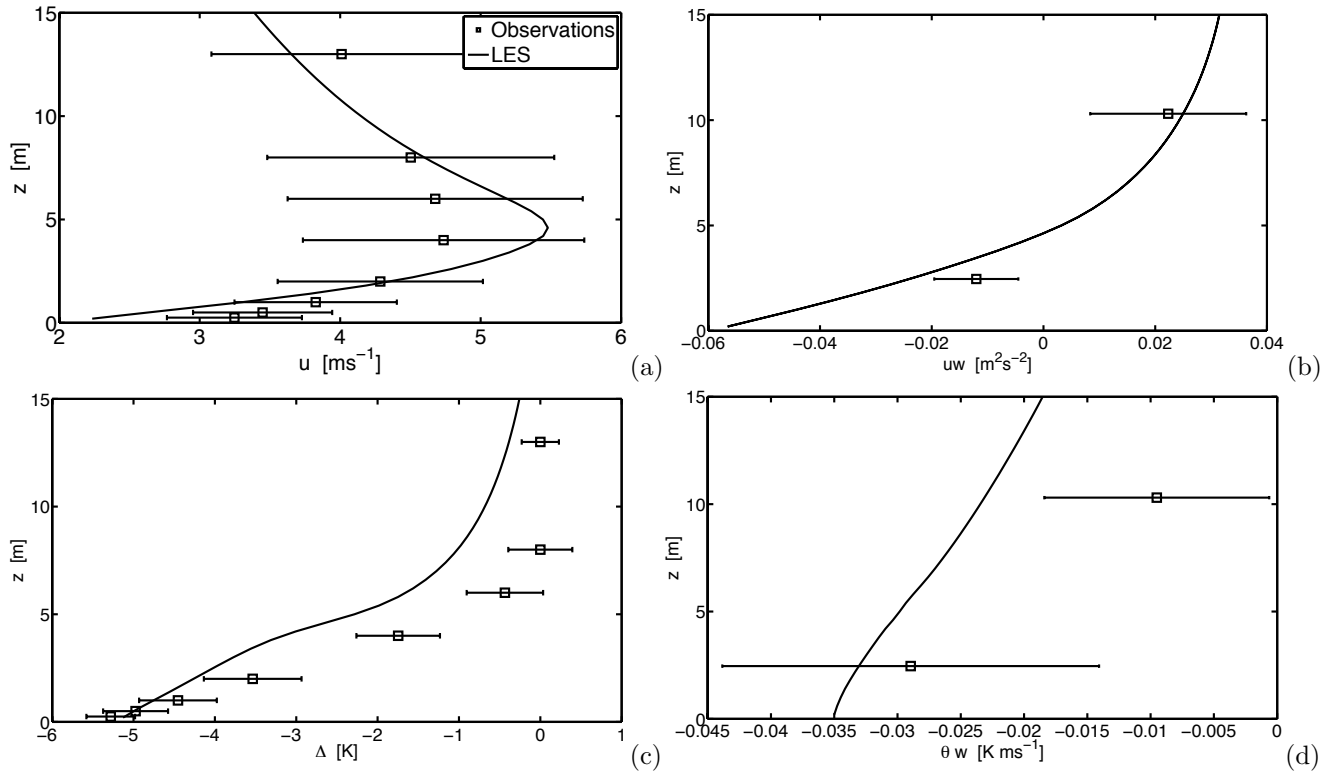


Figure 2: Comparison of model results to observations. (a) downslope velocity, and (b) vertical momentum flux, (c) temperature deficit, and (d) heat flux.

4 Sensitivity study

In the numerical study of katabatic flow by Nappo and Rao (1987), the effect of the ambient stratification on steady katabatic flow was investigated. Simulations using two different lapse

rates, $\gamma = 0.1$ and $\gamma = 10$, K km⁻¹ showed that the flow was considerably weaker and shallower for the strong stratification case. One of the focuses of this study is to further investigate the effect of stratification on the flow. The near-surface stratification is in turn influenced by the

Table 1: Summary of input parameters in numerical simulations.

Simulation	N [$10^{-2} s^{-1}$]	$\overline{wb_s}$ [$10^{-3} m^2 s^{-3}$]	α [degrees]
G1F1A2	1.01	1.02	5.0
G1F2A1	1.01	1.36	3.5
G1F2A2	1.01	1.36	5.0
G1F2A3	1.01	1.36	6.5
G1F2A4	1.01	1.36	7.5
G1F3A2	1.01	1.70	5.0
G2F1A1	1.24	1.02	3.5
G2F1A2	1.24	1.02	5.0
G2F1A3	1.24	1.02	6.5
G2F2A1	1.24	1.36	3.5
G2F2A2	1.24	1.36	5.0
G2F2A3	1.24	1.36	6.5
G3F1A2	1.43	1.02	5.0
G3F2A2	1.43	1.36	5.0
G3F3A2	1.43	1.70	5.0
G4F1A2	1.60	1.02	5.0

surface buoyancy flux, and will in the following also be addressed. The effect of a third parameter, the slope-angle α , will be discussed separately.

16 numerical simulations have been carried out with Brunt-Väisälä frequencies ranging from ~ 1 to $1.6 \cdot 10^{-2} s^{-1}$, surface buoyancy fluxes ranging from ~ 1 to $1.7 \cdot 10^{-3} m^2 s^{-3}$, and α ranging from 3.5° to 7.5° ; a summary of the input parameters used is given in Table 1.

Figure 3(a) shows the down-slope velocity profiles of a selection of the simulations; the selection includes the extreme input parameters in background stratification and surface forcing. As expected, the velocity decreases with increasing background stratification (G1F1A2 and G4F1A2), and increases with increasing surface buoyancy flux (G1F1A2 and G1F3A2). For the wind maximum height z_j , there is an inverse relation; z_j decreases for increasing N , but increases for decreasing $\overline{wb_s}$. Turning to the buoyancy profiles, we see in Figure 3(b) that all profiles tend to zero far away from the surface; near the surface it would appear that the background stratification has a smaller impact on the buoyancy than the surface buoyancy flux, but such a conclusion can only be made after finding proper

scaling parameters. Such scale factors for velocity, buoyancy and length are derived from the equations Prandtl based his model on:

$$b \sin \alpha - \frac{\partial \overline{wu}}{\partial z} = 0,$$

$$-uN^2 \sin \alpha - \frac{\partial \overline{wb}}{\partial z} = 0,$$

(Prandtl, 1942; Shapiro and Fedorovich, 2008). In the momentum equation the buoyancy acceleration is opposed by the turbulent stress, and in the buoyancy equation heating by advection of ambient air is opposed by surface cooling. By introducing the generic scales V (velocity), L (distance) and B (buoyancy), the equations can be recast on the form

$$b_n + \frac{1}{\sin \alpha} \frac{V^2}{LB} \frac{\partial \tau_n}{\partial z_n} = 0, \quad (5)$$

$$u_n + \frac{1}{\sin \alpha} \frac{B}{LN^2} \frac{\partial Q_n}{\partial z_n} = 0, \quad (6)$$

where the subscript n denotes non-dimensionalized variables: $z_n = z/L$, $b_n = b/B$, $\tau_n = \overline{uw}/V^2$ and $Q_n = \overline{wb}/(VB)$. The two external parameters N and $F_s = \overline{wb_s}$, can be combined to give the units of length, velocity and buoyancy. (To obtain positive scales, the absolute value of the surface buoyancy is used.) Following Schumann (1990), and Shapiro and Fedorovich (2008) we get

$$V_1 = F_s^{1/2} N^{-1/2}, \quad B_1 = F_s^{1/2} N^{1/2} \quad \text{and} \\ L_1 = F_s^{1/2} N^{-3/2}. \quad (7)$$

Figure 3(c) shows that the scaled down-slope velocity profiles converge only for $z/L_1 \gtrsim 0.2$ and that the heights of the wind maxima do not coincide. The wind maxima are brought a bit closer together, especially the wind maxima of the simulations G1F1A2 and G1F3A2. Figure 3(d) shows that the scaled buoyancy profiles also only converge for $z \gtrsim 0.2$, and that near the surface the scaling does not bring the buoyancy profiles closer together.

We have also consider scales involving the height of the wind maximum, z_j , which is determined by the flow, e.g.

$$V_2 = F_s N^{-2} z_j^{-1} \quad \text{and} \quad B_2 = F_s N^{-1} z_j^{-1}. \quad (8)$$

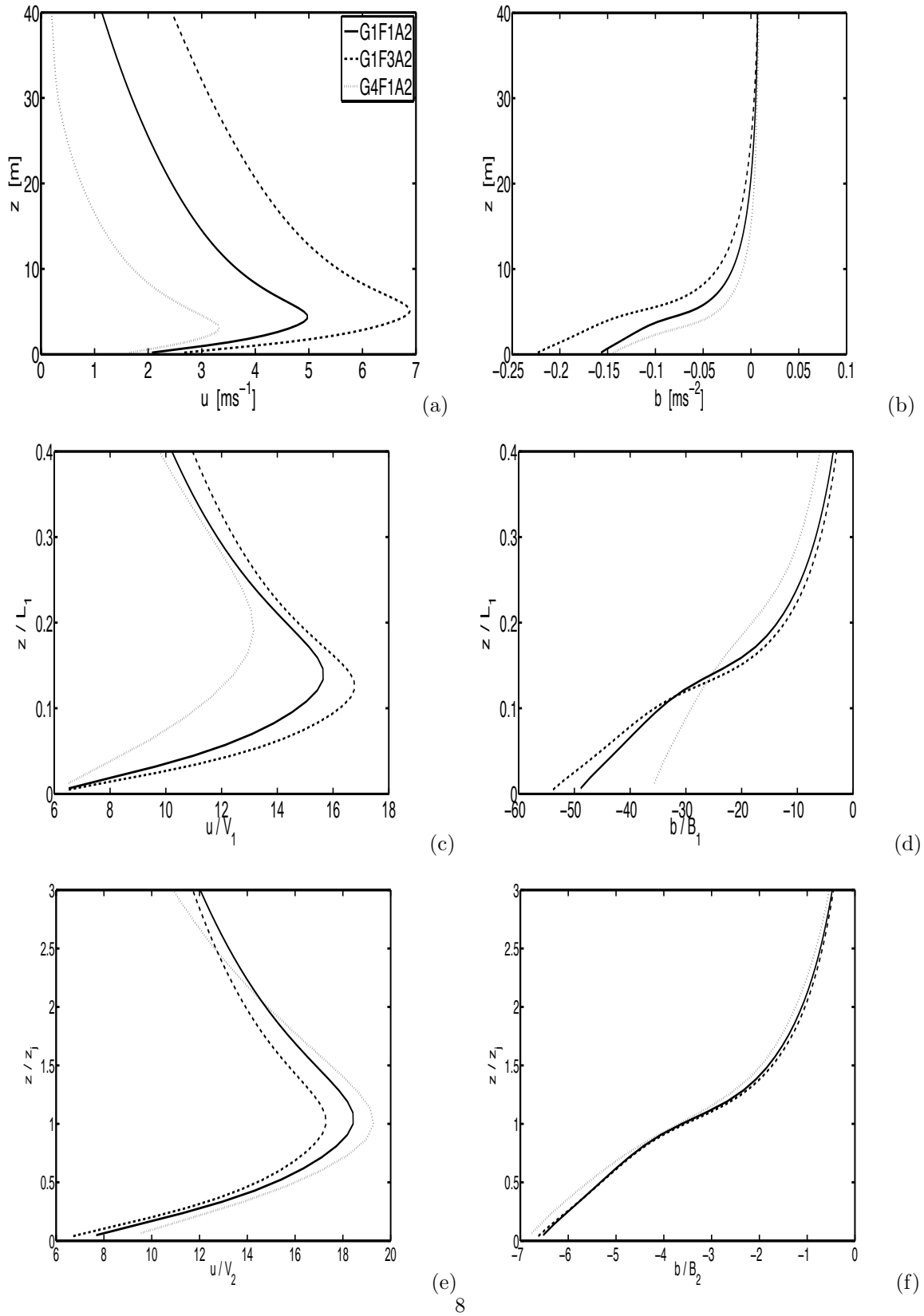


Figure 3: Dimensional down slope velocity (a), buoyancy (b), and scaled velocity (c,e), buoyancy (d,f). See text for details.

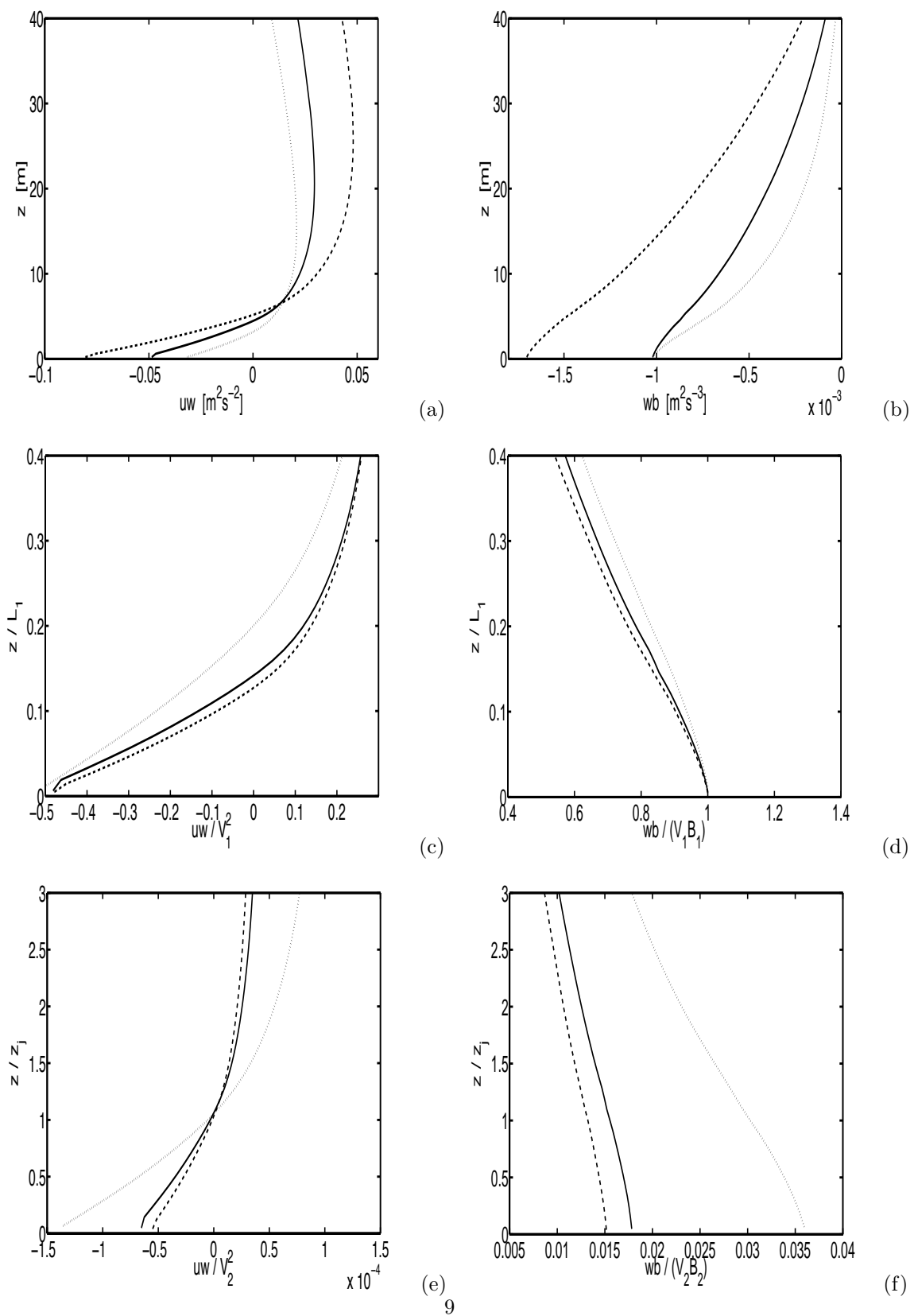


Figure 4: Dimensional (a) and scaled (b) momentum flux, in (c) and (d) dimensional and scaled buoyancy flux. Legends as in Figure 3.

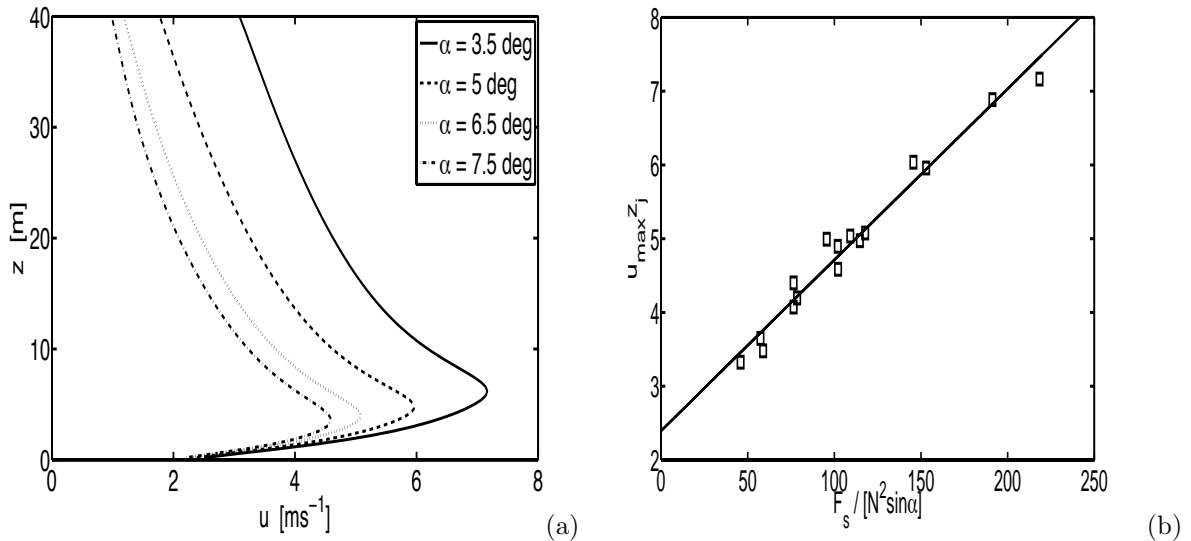


Figure 5: Down-slope velocity simulations with different α (a), and $u_{\max} z_j$ as function of $F_s / (N^2 \sin \alpha)$; straight line is linear regression.

The scaled down-slope velocities are shown in Figure 3(e); by scaling the height by z_j , the heights of the wind maxima will by definition all coincide at $z/z_j = 1$, but we also note that the magnitude of the velocity maxima are brought closer together when scaling \bar{u} by V_2 . The flow-dependent scaling parameters also work well for the buoyancy profiles, Figure 3(f); upon scaling \bar{b} by B_2 all buoyancy profiles practically fall onto one curve.

Next we consider the dimensional and scaled fluxes of momentum and buoyancy, Figure 4. The profiles of the dimensional momentum fluxes vary at all heights; below the wind maximum they are negative and increase until $z \sim 15 - 25$ m. At the height of the wind maximum the momentum fluxes go to zero; the intersection of all curves near $z \sim 6$ m is merely a coincidence, other simulations do not pass through that intersection point. The dimensional buoyancy flux profiles, Figure 4(b), go from F_s at the surface to zero at the boundary top, not linearly as in the SBL over flat surfaces (Nieuwstadt, 1984), but somewhat curved. Figures 4(c,d) show the momentum and buoyancy fluxes scaled by respectively V_1^2 and

$V_1 B_1$. Two of the three scaled momentum flux profiles coincide to a good degree, the 'outlier' is simulation G4F1A2. The \overline{wb} profiles are scaled by $V_1 B_1 = F_s$; near the surface all scaled buoyancy flux profiles go to unity, further away a small spread between the scaled profiles is observed. Lastly we scale the momentum and buoyancy flux profiles by respectively V_2^2 and $V_2 B_2$, Figures 4(e,f). Because the height has been scaled by z_j , all scaled momentum flux profiles go to zero at $z/z_j = 1$. We further note that two of the three profiles shown coincide to a good degree; the 'outlier' is the G4F1A2 simulation which differs from the other two in the background stratification. Scaling the buoyancy flux profiles with $V_2 B_2$ clearly does not bring the scaled flux profiles closer together.

The slope-angle α is the last variable we will focus on. Figure 5(a) shows the down-slope velocity profiles of four simulations with fixed N and F_s but with varying α ; both the magnitude of the wind maximum u_{\max} , and z_j increase with decreasing slope-angle. Schumann (1990), who performed numerical simulations with various slope-angles, found for the anabatic flow over moderately steep slopes that the wind

maximum only weakly depends on α . He related the vertically averaged down-slope velocity to the slope-angle by $UD h = F_s/(N^2 \sin \alpha)$, the right hand side being very similar to the scale factor V_2 . From the Prandtl model a similar relation for the product $u_{max} z_j$ can be found:

$$u_{max} z_j = \frac{\pi e^{-\pi/4}}{2\sqrt{2}} \frac{F_s}{N^2 \sin \alpha}.$$

Figure 5(b) confirms the relation, although the linear regression coefficient is different (0.19). Note that the linear regression was obtained using all simulations, when isolating simulations with constant $F_s N^{-2}$ but varying α , the regression coefficient was 0.25. We would expect $u_{max} z_j$ to vanish for small $F_s/(N^2 \sin \alpha)$, but this is not verified in the figure.

5 Discussion

A relation between the two length scales introduced in the previous section, L_1 and z_j , is sought; Figure 6 shows that z_j increases linearly with L_1 . Of the nine simulations having $\alpha = 5^\circ$, four have the same wind maximum height, most likely because z_j is determined on a discretized grid. For instance, the height of the wind maximum is typically around $z \sim 4$ m, and with a vertical grid distance $\delta_z = 40$ cm, 'moving' z_j up or down one grid level gives a relative change of 10%. We take this discretization problem into account when doing a linear regression analysis; the regression coefficients for $\alpha = 3.5^\circ$, 5° and 6.5° are respectively 0.12, 0.08 and 0.06. For the moderately steep slopes that we have simulated, we conclude that the increase in z_j for increasing L_1 is smaller for large α than for small α . Further analysis must determine how the regression coefficients varies with F_s , N and α .

6 Conclusion

Slope flows over cool, inclined surfaces have been studied using large-eddy simulations with rotated coordinate system. Periodic boundary conditions have been applied to the velocity

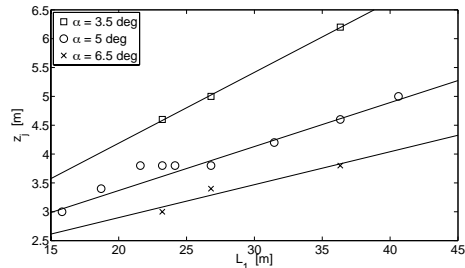


Figure 6: z_j as function L_1 .

components, temperature deficit and the sub-filter scale turbulent kinetic energy, and simulations are run until steady state. Model validation with *in-situ* observations from an Alpine glacier show good agreement between modelled and observed down-slope velocity and momentum flux, but suggests that the boundary layer depth is overestimated.

The sensitivity study where the external parameters α , N and F_s shows that the down-slope velocity increases with increased surface buoyancy flux, but decreases with increased stratification and slope-angle. Two sets of scaling parameters for the velocity, buoyancy and height have been introduced, one set is based solely on external parameters, and one set on the height of the wind maximum, z_j . We have seen that the mean profiles of the down-slope velocity and buoyancy scale well the z_j dependent parameters.

Fluxes of momentum and buoyancy have also been studied as function of N and F_s . Momentum fluxes are negative below the wind maximum, go to zero at z_j and continue increasing up to 3-4 times the height of the wind maximum, where after momentum fluxes start diminishing again. The buoyancy profiles are similar to the buoyancy profiles in the SBL over flat surfaces, but due to the advection of upslope ambient air, the decrease in \overline{wb} is not linear but curved. The scaled profiles of respectively momentum and buoyancy, show that the scale parameters solely based on external parameters work the best.

Analysis has further shown a linear relation between z_j and L_1 , in the future we will pursue a theoretical reasoning for the relation based on the Prandtl model. Also, with the aid of LES

it is now possible to study the scaling behavior of the various terms in the TKE budget, and determine how exchange coefficients of momentum and buoyancy, and thus also the Prandtl number, vary with height.

References

- Beare, R. J. *et al.* 2006. An intercomparison of large-eddy simulations of the stable boundary layer. *Boundary-Layer Meteorol.*, **118**, 247–272 .
- Cuijpers, J. 1994. *Large-eddy simulation of cumulus convection*. Ph.D. thesis, IMAU, Utrecht University.
- Deardorff, J. W. 1980. Stratocumulus-capped mixed layers derived from a three-dimensional model. *Boundary-Layer Meteorology*, **18**, 495–527.
- Delage, Y. 1974. A numerical study of the nocturnal atmospheric boundary layer. *Quart.J.Roy.Meteorol.Soc.*, **100**, 351–364.
- Denby, B. 2002. Second-order modelling of turbulence in katabatic flows. *Boundary-Layer Meteorol.*, **103**, 459–468.
- Dosio, A. 2005. *Turbulent dispersion in the Atmospheric Convective Boundary Layer*. Ph.D. thesis, Wageningen University.
- Fleagle, R. G. 1950. A theory of air drainage. *J. Meteor.*, **7**, 227–232.
- Foken, T. 2006. 50 years of the Moning-Obukhov similarity theory. *Boundary-Layer Meteorol.*, **119**, 431–447.
- Geurts, B. J. 2004. *Elements of direct and large-eddy simulation*. Philadelphia, New York.
- Greuell, W., Knap, W., and Smeets, P. 1997. Elevation changes in meteorological variables along a midlatitude glacier during summer. *J.Geophys.Res.*, **102**, 941–954.
- Grisogono, B. 2003. Post-onset behaviour of the pure katabatic flow. *Boundary-Layer Meteorol.*, **107**, 157 – 175.
- Grisogono, B. and Oerlemans, J. 2001a. Katabatic flow: Analytic solution for gradually varying eddy diffusivities. *J.Atmos.Sci.*, **58**, 3349 – 3354.
- Grisogono, B. and Oerlemans, J. 2001b. A theory for the estimation of surface fluxes in simple katabatic flows. *Quart.J.Roy.Meteorol.Soc.*, **127**, 2725 – 2739.
- Gutman, L. N. and Malbakhov, V. M. 1964. On the theory of katabatic winds of antarctica. *Met. Issled*, **9**, in Russian 150 – 155.
- Haiden, T. and Whiteman, C. D. 2005. Katabatic flow mechanisms on a low-angle slope. *J.Appl.Meteorol.*, **44**, 113–126.
- Kavcic, I. and Grisogono, B. 2007. Katabatic flow with coriolis effect and gradually varying eddy diffusivity. *Boundary-Layer Meteorol.*, **125**, 377 – 387.
- Khairoutdinov, M. and Randall, D. A. 2003. Cloud resolving modeling of the ARM summer1997 IOP: Model formulation, results, uncertainties, and sensitivities. *J. Atmos. Sci.*, **60**, 607–625.
- Mahrt, L. 1998. Stratified atmospheric boundary layers and breakdown of models. *Theoret. Comput. Fluid Dynamics*, **11**, 263–279.
- Mahrt, L. 1999. Stratified atmospheric boundary layers. *Boundary-Layer Meteorol.*, **90**, 375–396.
- Manins, P. C. and Turner, J. 1978. The relation between flux ratio and energy ratio in convectively mixed layers. *Quart. J. Roy. Meteor. Soc.*, **104**, 39–44.
- Nappo, C. and Rao, K. 1987. A model study of pure katabatic flows. *Tellus*, **39A**, 61–71.
- Nappo, C. J. 2002. *An introduction to atmospheric gravity waves*. Academic Press.
- Nieuwstadt, F. 1984. The turbulent structure of the stable nocturnal boundary layer. *J.Atmos.Sci.*, **41**, 2202–2216.

- Oerlemans, J. 1994. Quantifying global warming from retreat of glaciers. *Science*, **264**, 243–245.
- Papadopoulos, K. H., Helmis, C. G., Soilemes, A. T., Kalogiros, J., Papageorgas, P. G., and Asimakopoulos, D. N. 1997. The structure of katabatic flows down a simple slope. *Quart.J.Roy.Meteorol.Soc.*, **123**, 1581–1601.
- Parmhed, O., Oerlemans, J., and Grisogono, B. 2004. Describing surface fluxes in katabatic flow on Breidamerkurjökull, Iceland. *Quart.J.Roy.Meteorol.Soc.*, **130**, 1137–1151.
- Pope, S. B. 2000. *Turbulent Flows*. Cambridge University Press.
- Prandtl, L. 1942. *Führer durch die Strömungslehre*. Vieweg u. Sohn, Braunschweig.
- Raasch, S. and Etling, D. 1991. Numerical simulation of rotating turbulent thermal convection. *Beitr. Phys. Atmos.*, **64**, 185–199.
- Riley, K. F., Hobson, M. P., and Bence, S. 1997. *Mathematical methods for physics and engineering*. Cambridge University Press.
- Sagaut, P. 1998. *Large-Eddy Simulation for Incompressible Flow*. Springer. 319pp.
- Schumann, U. 1990. Large-eddy simulation of the up-slope boundary layer. *Quart. J. Roy. Meteorol. Soc.*, **116**, 637–670.
- Shapiro, A. and Fedorovich, E. 2008. Coriolis effects in homogeneous and inhomogeneous katabatic flows. *Quart.J.Roy.Meteorol.Soc.*, **134**, 353 – 370.
- Skyllingstad, E. D. 2003. Large-eddy simulation of katabatic flows. *Boundary-Layer Meteorol.*, **106**, 217–243.
- Van den Broeke, M. 1997. Momentum, heat, and moisture budgets of the katabatic wind layer over a midlatitude glacier in summer. *J.Appl.Meteorol.*, **36**, 763–774.
- Van den Broeke, M., van Lipzig, N., and van Meijgaard, E. 2002. Momentum budget of the East-Antarctic atmospheric boundary layer: results of a regional climate model. *J.Atmos.Sci.*, **59**, 3117–3129.